Synthesis and Characterization of NMC622 Cathode Material Modified by Various Cheap and Abundant Transition Metals for Li-ion Batteries

Anisa Raditya Nurohmah
Department of Chemical Engineering, Universitas Sebelas Maret

Ayuningtyas, Megadita
Department of Physics, Faculty of Mathematic and Natural Science, Universitas Sebelas Maret

Cornelius Satria Yudha
Department of Chemical Engineering, Universitas Sebelas Maret

Purwanto, Agus
Department of Chemical Engineering, Universitas Sebelas Maret

他

https://doi.org/10.5109/4794168

出版情報：Evergreen. 9 (2), pp.427-437, 2022-06. 九州大学グリーンテクノロジー研究教育センター
バージョン：

Synthesis and Characterization of NMC622 Cathode Material Modified by Various Cheap and Abundant Transition Metals for Li-ion Batteries

Anisa Raditya Nurohmah[1], Megadita Ayuningtyas[2], Cornelius Satria Yudha[1,3], Agus Purwanto[1,3], and Hendri Widiyandari[2,3]*

[1]Department of Chemical Engineering, Universitas Sebelas Maret, Surakarta, Indonesia;

[2]Department of Physics, Faculty of Mathematic and Natural Science, Universitas Sebelas Maret, Surakarta, Indonesia

[3]Centre of Excellence for Electrical Energy Storage, Universitas Sebelas Maret, Surakarta, Indonesia

*Author to whom correspondence should be addressed:
Email: hendriwidiyandari@staff.uns.ac.id

(Received December 7, 2021; Revised June 1, 2022; accepted June 1, 2022).

Abstract: The lithium-ion battery is the most advanced battery technology widely available. Lithium rechargeable batteries have recently been used in transportation (for example, electric cars) and energy storage systems that need a lot of energy and power on a large scale. $LiNi_{0.6}Mn_{0.2}Co_{0.2}O_2$ (NMC622) is a cathode material that has a high energy density. Doping in lithium-ion battery cathode materials has become a topic of interest worldwide. In this study, NMC622 cathode synthesis was conducted with transition metal doping using co-precipitation. The co-precipitation approach was chosen for the material's production $(LiNi_{0.6}Mn_{0.2}Co_{0.2}O_2)_{1-x}M_x$ (M = Fe, Ti, Zn, Ce, and Cu) because of its ability to produce particles with a high degree of atomic uniformity. Due to the high energy metal oxygen bond dissociation, Fe, Ti, Zn, Ce, and Cu were utilized as doping materials in this work. Oxalic acid was used as a precipitation agent, and ammonia was used as a chelating agent. The doping metal used was precipitated using oxalic acid. NMC622 which has been precipitated into NMC622 precursor and doped metal that has been precipitated is mixed for later solid-state processing. Under the flow of air, the obtained oxalate precursor is heated. The characterization of metal-doped NMC622 was carried out. The x-ray diffraction pattern depicts the hexagonal layered material's structure. FTIR analysis confirmed the missing C-O bonds of the obtained product. SEM (scanning electron microscope) studies show a polyhedral morphology of the material. A charge-discharge test at 1/10 C between 2.6 and 4.3 V was used to achieve the electrochemical performance. Ce doping resulted in the best specific capacity and could be compared with non-doped materials.

Keywords**:** Battery, Cathode, NMC622, Doping

1. Introduction

Energy is a component that people needed at all times throughout their lives since basically

all activities, including transportation, rely on its availability. The use of cars with fossil fuels has begun to be replaced with electric cars that are more practical and environmentally friendly. Applications in energy storage in electric cars such as batteries are increasing in use. Energy storage in the form of electrical devices must be efficient, lightweight, not oversized, which had excellent performance to keep up with its development.

One of the solution is lithium ion batteries (LIBs) which has the advantage of high performance in charge-discharge process, high energy density, no memory effect, good cyclability and the possibility of small self-discharge [1,2)]. LIBs have been used in both small and medium-sized electricity storage systems [3)]. LIBs are a type of rechargeable secondary battery. Therefore, nowadays LIBs are widely used for various electronic items such as: laptops, cameras, electric bicycles and even being developed for electric cars because they have high energy density, high working potential, and long service life [4)]. Due to the possibility of lithium dendrite formation, lithium ion batteries do not use lithium metal as an anode in principle[5)]. Because of their flexible form and lengthy usage life, batteries are regarded as the most effective and practical technology for powering electronic equipment[6)].

$LiCoO_2$ is a commercialized first-layer structured cathode. The use of this material began to be reduced because this material is considered expensive, toxic and can explode when used in extreme conditions [7]. $LiCoO_2$ has a high energy density, making it suited for smartphones and notebook computers, however due to their low crystal structure stability, they cannot be anticipated to have extended cycle lives or a high level of safety[8]. $LiNiMnCoO_2$ or usually called NMC has a much larger capacity than $LiCoO_2$ even with the same operating voltage. According to economic aspects, NMC has a cheaper price than $LiCoO_2$ due to the reduced amount of cobalt due to substitution. NMC is a lithium battery cathode material with several advantages, including high capacity, high heat and current stability, a large volume capacity, and a longer cycle life [9]. NMC is also have been combined with sodium to be used as cathode for Sodium Ion Batteries[10,11].

Recently, research on lithium-ion batteries has only become at the level of energy density, so there are no life-saving and safety concerns[12]. It is worshiped by a pair of both active ingredients of anode and cathode. Surviving the active ingredient in an exothermic reaction that is not controlled can mutate the battery of thermal escape cells. In cathode, the source of thermal runaway can be the production of highly reactive efficiency of phase changes at high temperatures and reactions with combustible electrolytes based on organic material [13]. Therefore, the power plant functional active ingredient cathode, which has high energy, such as lithium-nickel-manganese-cobalt-starch (NMC) is very highly active high-energy cathode material that is safe [14]. Some of the NMC materials that have been studied are NMC111 (Nickel, Cobalt, Manganese in a ratio of 1: 1:1), NMC442 (Nickel, Cobalt, Manganese in a ratio of 4:4:2) and NMC622 (Nickel, Cobalt, Manganese in a ratio 6:2:2).

One common method used to stabilize the active material of cathodes is doping. Doping, or the displacement of cations in the host structure, can change the crystal structure. The release of oxygen, which is an unavoidable phase during NMC structural degradation, is inhibited by high bond dissociation energy, which improves structural stability[15]. The element of doping that has been studied is Al [16–18], Mg[19], Ti [20], Cr [21], Mo [22], Nb [21], Sn[15,23] and Fe [17,24,25]. Due to the presence of electrochemically inert doping materials, the release capacity decreases as the concentration of doping elements increases [23], while structural stability improved [17,20,22,24,26]. Primary doping occurs through substitution of Co by other elements, due to some of Co's weaknesses such as political and economic unstable production countries, as well as exorbitant prices. In addition, Ni or Mn substitutions are not studied because Ni produces high capacity and Mn maintains thermal stability[14]. Hongyang stated that cobalt has little impact on the quality of LIBs with nickel-rich material[27].

The choosing of doping is according to the high energy of metal-oxygen bond dissociation. Fe, Ti, Zn, Ce, and Cu are transition metals with a high dissociation energy and are relatively simple to obtain in intriguing qualities to examine. There has been previous research that has used Fe as a doping element. Wilcox synthesizes $Li(Ni_{0.4}Co_{0.15}Fe_{0.05}Mn_{0.4})O_2$ using combustion method with glycine nitrate. Cells using $Li(Ni_{0.4}Co_{0.15}Fe_{0.05}Mn_{0.4})O_2$ recyclable cathode show reduced efficiency relative to $Li(Ni_{0.4}Co_{0.15}Fe_{0.05}Mn_{0.4})O_2$ whereas iron must be electroactive in the operating voltage range of 4.3V and no increased impact [17]. Park also used Fe as a doping element to synthesize $LiNi_{1/3}Co_{1/3}Mn_{1/3}Fe_x(OH)_2$ from a lithium ion battery that had been used and used hydroxide precipitation [24]. Fe^{3+} ions can be found in interstice locations or within the lattice in iron, making it one of the best doping materials[28]. The Ti metal has also been researched as doping on the NMC442 cathode and shows that with doping it could increase discharge capacity and decrease capacity in high pressure conditions[29].

Materially, Markus et.al researched that with Ti doping can improve the stability of NMC structures by strengthening formation energy and also bonding with oxygen [30]. Zn metal is used as doping on NMC111 cathode using sol-gel method indicating absence of crystal structure and morphological changes [31]. ZnO also used as composite material for lithium ion battery electrolyte[32]. Ce in the form of CeO_2 has been used as a coating on NMC111 batteries [33]. Cu metal has also been used as doping on the NMC111 cathode with sol-gel method showing that Cu doping produces better electrochemical performance compared to NMC111 without doping and in the presence of doping Cu can help lower the degree of mixing cation [34]. NMC622 will have a better prospect than NMC111 due to its lower cobalt content.

Some of the above metals have never been used as doping on NMC622 cathodes. In this study, NMC622 cathode synthesis was conducted with transition metal doping using co-precipitation method which is also a novelty in this study. NMC622 synthesis uses a co-precipitation process with oxalic acid stifling agents that has not been performed by previous research.

2. Materials and Methods

2.1.Materials

Materials used is nickel sulfate from Zenith (Brazil), manganese sulfate from Y.C. Chemicals (China), cobalt sulfate from Rubamin (India), as doping material; iron sulfate, titanium dioxide, zinc sulfate, cerium dioxide, copper sulfate and magnesium sulfate. Additional ingridients are oxalic acid, ammonia, lithium hydroxide from Leverton (India), PVDF (polyvinylidene fluoride, MTI, America), AB (acetylene black), KS6, and NMP(N-Methyl-2-pyrrolidone).

2.2.Methodology

2.2.1. Synthesis of NMC precursor

Nickel sulfate, manganese sulfate, cobalt sulfate with a molar ratio of Ni^{2+}: Mn^{2+}: Co^{2+} equals to 6:2:2 were mixed in aquadest to get 1 M solution and stirred at 60ºC while waiting for a homogenous solution was formed. 2M ammonia solution was added and agitated for 30 minutes at 60ºC. The pH was adjusted to 2 by adding a 2M oxalic acid solution, which was then agitated for 2 hr. The slurry was filtered, and the precipitate was washed repeatedly up to the pH was balanced. The precipitate was dried for 12 hours at 100°C in an oven. This substance has been identified as a precursor of NMC.

2.2.2. Synthesis of Metal Doped Oxalate

1 molar of iron sulfate were mixed with 1 molar of oxalic acid solution in a one-to-one molar ratio until a homogenous solution was formed. The pH of the solution was adjusted by filtering and rinsing until it was neutral. Same method was done for other variations of metal doping (titanium dioxide, zinc sulfate, cerium dioxide, copper sulfate and magnesium sulfate). Iron oxalate, zinc oxalate, magnesium oxalate, titanium oxalate, and cerium oxalate were ready to use as doping materials after being dried in an oven overnight.

2.2.3. Synthesis of NMC cathode

The NMC precursor was blended and combined with lithium hydroxide (Leverton, India) with a 5% excess due to NMC moles and doping components (iron oxalate, zinc oxalate, magnesium oxalate, titanium oxalate, and cerium oxalate) using a porcelain mortar and pestle. In an oxygen atmosphere, the material was sintered for 12 hours at 900ºC.

2.2.4. Characterization of NMC cathode

SEM (Scanning Electron Microscopy), XRD (X-Ray Diffractometer), and FTIR (Fourier Transform Infrared Spectroscopy) were used to investigate the materials' morphology, crystallinity, and functional group. The morphology of the material was analyzed using SEM Jeol JSM-6510LA, Tokyo, Japan. The crystal structure of the products was analyzed using an EQ-MD-10-LD Precision Mini XRD employing CuKα radiation λ = 1.54 ´Å with a 2θ range of 10–80◦ and scan-rate of 0.02◦ per second. The functional group of the material was examined using Shimadzu FTIR Spectrometer, Japan with mid-IR region (4000–400/cm). The best synthesis product was then put through battery performance testing depending on the characterization results. Following that, the coating is prepared by putting PVDF in the dry oven and AB, KS6, and the NMC Doped sample in the wet oven. In NCA: AB: KS6: PVDF, all of the materials are mixed in a 92:1.5:1.5:5 ratio. The cathode sheet is then created using a coating equipment and dried in a vacuum oven. The capacity test of NMC Doped batteries must be examined.

3. Results and Discussion

Various metal doping compositions, such as Fe, Ti, Zn, Ce, Cu, and Mg, were used to synthesize $Li(Ni_{0.6}Mn_{0.2}Co_{0.2})_{1-x}M_xO_2$ samples. Mg which is an alkaline metal was used as a comparison in this study. All doping metals have previously been precipitation using oxalic acid to maximize the solid-state process with NMC622. With the presence of doping this metal also supports the reduction of expensive and toxic cobalt materials. There were 19 samples in this experiment: pure NMC622 (without doping), NMC622 with various metal doping (concentrations of 1%, 3%, and 5%).

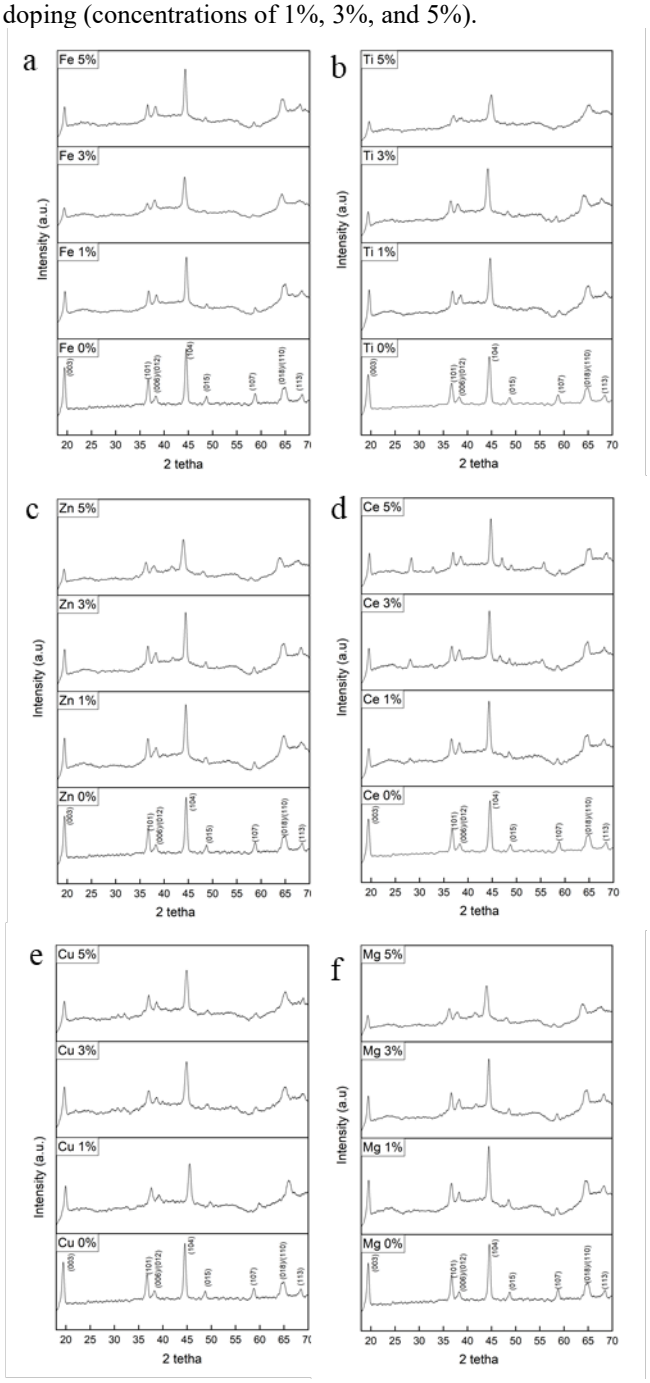

Fig. 1: NMC622 Cathode XRD Results with Various Doping (a. Fe, b. Ti, c. Zn, d. Ce, e. Cu, f. Mg)

Fig. 1 shows the NMC622 XRD pattern with various doping. As can be seen in Fig. 1, practically all samples have peaks that are identical to pure NMC622 (without doping), sharp peak and well defined, indicating that the crystallization of the produced materials is good. Except from peaks between 20.5 and 22, other peaks in The XRD pattern corresponds to the a-NaFeO2 structure with space room group R3m[35]. Weak peaks at 20.7 and 21.8 can be explained to diffraction (020) and (110) in Li_2MnO_3 components[36,37]. These results confirm that NMC622 with various doping materials is a combination of monoclinic and hexagonal Li_2MnO_3(C2/m) components of monoclinic and hexagonal $LiMO_2$(R3m)[38]. Furthermore, adding metal doping to the material will result in minor XRD pattern modifications.

For Mg, Ti and Zn, when the doping concentration is 5%, near 42.5-44, a very faint peak occurs. This peak became clearer and an additional peak approaching 62-64 was also formed when doping was less than 5%. Sharp peaks at angles 2theta 15-20° and 40-46° indicate that NMC622 material has high crystalline properties[39]. However, for NMC622 Ce-doped is almost the same for all concentrations, but has a new peak at an angle of 2θ 28-30° and becomes higher with an increase in Ce concentration, which indicates the presence of a CeO_2 phase[33,40]. This is important because of the fact that most Ce elements can be substituted for transition metal elements in the lattice of layered oxide materials [41]. According to the XRD results in Fig. 1, it can be concluded that doping of iron, titanium, iron, zinc, copper and magnesium was successfully performed without the secondary phase being detected. From Fig. 1, we can specify the grid parameters (c/a), coefficient R, ratio I(003)/I(104) and crystal diameter listed in Table 1.

The values c and a for hexagonal structure can be obtained using the least square regression approach as follows:

$$n\lambda = 2d\sin\theta \quad (1)$$

with:

d	crystal distance
sin(θ)	diffraction angle
λ	X-ray wavelength
n	sequence of reflections (positive integers)
θ	angle between wave vector of incident wave (°)

$$\frac{1}{d_{hkl}^2} = \frac{4}{3}\left(\left(h^2 + k^2 + hk\right) + l^2\left(\frac{a}{c}\right)^2\right)\frac{1}{a^2} \quad (2)$$

$$\frac{1}{d_{hkl}^2 l^2} = \frac{4}{3}\frac{1}{l^2 a^2}\left(h^2 + k^2 + hk\right) + \frac{1}{c^2} \quad (3)$$

The equation above has an identic shape with a regression equation y = mx + n, with

$$y = \frac{1}{d_{hkl}^2 l^2}; x = \frac{4}{3}\frac{1}{l^2}\left(h^2 + k^2 + hk\right), m = \frac{1}{a^2}; n = \frac{1}{c^2} \quad (4)$$

The grid parameter's c/a value is a direct measure of the perfect grid deviation. Ratio c/a =4,899 is the ideal ratio obtained when the oxygen anion lattice has symmetrical $\sqrt{24}$ closed cubic packed[42]. The bigger c/a ratio shows a further constructed layered structure and easier Li ion transmission, as the ideal closed cubic packed grid has a value of c/a 4.899[43]. From Table 1, we may deduce that not every sample has a c/a greater than 4,899. The c/a value of pure NMC622 material (without doping) is 4.9275. This indicates that the material has a layered structure that enables it to effectively distribute and transmit Li ions. The c/a value of NMC622 changes after the doping process. The c/a can fluctuate based on the composition and type of dopant, as illustrated in Fig. 1.

Table 1. Lattice Parameter Value (c/a), Coefficient R, Intensity Ratio I(003)/I(104)

Sample	Lattice Parameter (c/a)	Coefficient R	Intensity Ratio I(003)/I(104)
NMC622 without doping	4.927	0.366	0.883
Fe 1%	5.402	0.344	0.587
Fe 3%	5.434	0.372	0.621
Fe 5%	5.411	0.383	0.555
Ti 1%	4.883	0.446	0.617
Ti 3%	4.758	0.461	0.439
Ti 5%	4.776	0.553	0.491
Zn 1%	4.915	0.366	0.649
Zn 3%	4.903	0.409	0.508
Zn 5%	4.892	0.448	0.457
Ce 1%	4.708	0.398	0.463
Ce 3%	4.748	0.432	0.559
Ce 5%	4.898	0.375	0.574
Cu 1%	5.264	0.421	0.721
Cu 3%	5.407	0.408	0.697
Cu 5%	5.408	0.393	0.563
Mg 1%	4.905	0.398	0.597
Mg 3%	4.789	0.389	0.577
Mg 5%	4.913	0.360	0.513

For most samples the composition of dopant Fe (1%, 3% and 5%), Zn (1%, 3%, and 5%), Ce 5%, Cu (1%, 3% and 5%), Mg 1%, and Mg 5%, c/a values more than 4.899. The above suggests that the material has a well-ordered layered structure that facilitates ion transport. Mixing cations between lithium and nickel ions in LIBs can degrade the electrochemical efficiency of lithium ion transfer-coated processes. The c/a number, on the other hand, falls below 4.899 for various dopant compositions. This indicates a less orderly layered structure and a better

Li-ions transport mechanism in this material. From the calculation stated in Table 1, Fe 3%, Ti 1%, Zn 1%, Ce 5%, Cu 5% and Mg 5% have higher c/a values.

The hexagonal structure of materials is related to the R coefficient. Hexagonal materials that have a lower R value are more ordered. Peak intensity values I(006), I(101), and I(102) are used to calculate the R coefficient. This peak can be obtained from Fig. 1 and calculated using equations (5).

$$R = \frac{I(006) + I(102)}{I(101)} \quad (5)$$

All samples exhibit R value of less than 0.45 except Ti 3% and Ti 5%, the lesser R value, the better the hexagonal form [44]. As other samples show, which shows almost all samples have the best conditions for making a good hexagonal structure of NMC622 material.

To determine the cause of the cation mismatch, The peak intensity ratios (003) and (104) can be calculated using the formula I(003)/I(104). This peak can be obtained from Fig.1. A higher ratio of I(003)/I(104) causes a decrease in cation mixing. The value of I(003)/I(104) must be more than 1.2 if the material is functioning properly [43]. According to Fig. 1, all samples had an I(003)/I(104) value of less than 1.2. As a result, all of these samples have the potential to interact cations. Each sample, however, has a distinct value for I(003)/I(104). The NMC622 Ti sample of 3% has the lowest I(003)/I(104) value. This means that this sample has the highest chance of mixing cations of any other sample. The NMC622 Cu sample of 1% has the highest I(003)/I(104) value. This means that of all the samples, this one has the least amount of cation mixing.

From the XRD test results, NMC622 with transition metal doping has a crystalline structure that is relatively the same as NMC622 without doping. In terms of lattice parameter analysis, most NMC622 materials with transition metal doping have values that are close to the ideal value for closed cubic packed material structures and higher than ideal values. So the results show that NMC622 material with transition metal doping has a stable structure that can prevent thermal runaway cell battery conditions. This is due to the selection of transition metals that have high oxygen bond dissociation energy so that the material structure is more stable.

Based on XRD analysis, each metal has the best dopant composition. Fe 5%, Ti 1%, Zn 1%, Ce 5%, Cu 5%, and Mg 5% have been selected because they have higher c/a and I(003)/I(004) values in their doping types. Furthermore, FTIR analysis of these materials is carried out. Fig. 2 shows the absorption spectrum of NMC622 cathodes with various doping compositions. The vibration of water molecules can be seen from large peaks of about 3340cm^{-1} and 1600cm^{-1} on the left side. The sharp peak located at about 1300cm^{-1} correlates with the C-O bond. Once excess lithium added, a precursor is prepared for sintering.

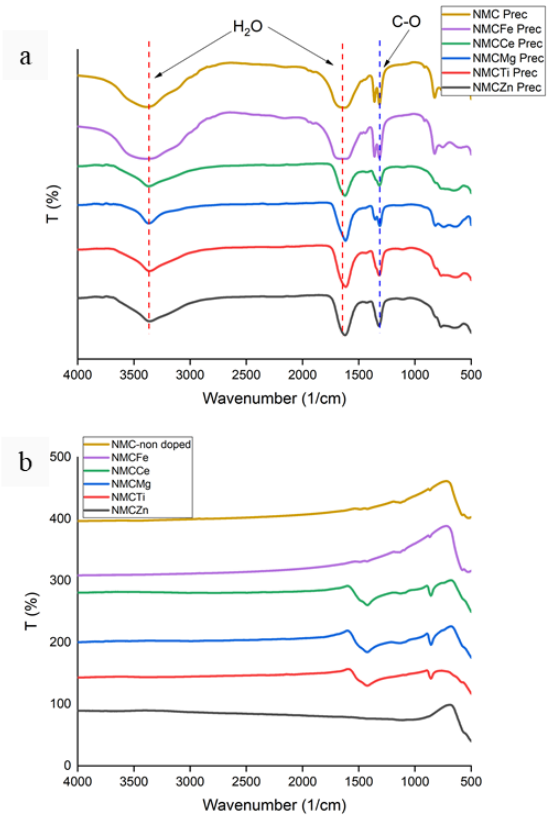

Fig. 2. FTIR Spectra from Precursors (a) and NMC622 Cathode Material with Various Doping (b)

After the sintering process, which can be seen on the right side, the water is lost. This can be utilized to answer that by sintering indicating the loss of bonds on the precursor as shown in Fig. 2b[45]. However, C-O bonds still remain slightly in NMC622 with Ti, Ce, Cu and Mg doping. NMC622 with Zn and Fe doping has lost its C-O bond, so for other materials it is necessary to find the best sintering conditions for losing C-O bonds.

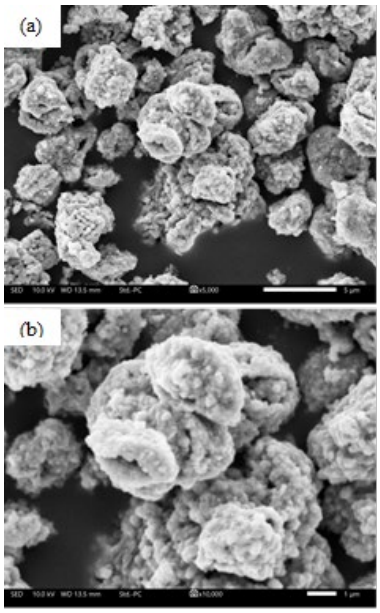

Fig. 3. SEM NMC622 Images Without Doping with

Magnification 5000x (a) and 10000x (b)

Table 2. Calculation of Secondary and Primary Particle Sizes in Micrometers (µm)

Material	Secondary Particle		Primary Particle	
	Size Range (µm)	Average Size (µm)	Size Range(µm)	Average Size (µm)
NMC622 Zn	2.59-6.07	3.93	0.16-0.71	0.42
NMC622 Ti	1.32-5.32	2.75	0.27-0.64	0.44
NMC622 Mg	0.90-3.50	1.95	0.27-0.82	0.46
NMC622 Ce	1.48-6.76	2.85	0.18-0.57	0.30
NMC622 Fe	1.35-6.09	3.47	0.20-1.02	0.51
NMC622 Cu	1.09-4.58	1.97	0.27-0.71	0.41

Fig. 3 shows the results of SEM NMC622 at magnifications of 5000 and 10000. NMC622 without doping has a primary particle size in the range of 1.35-8.07 micrometers.

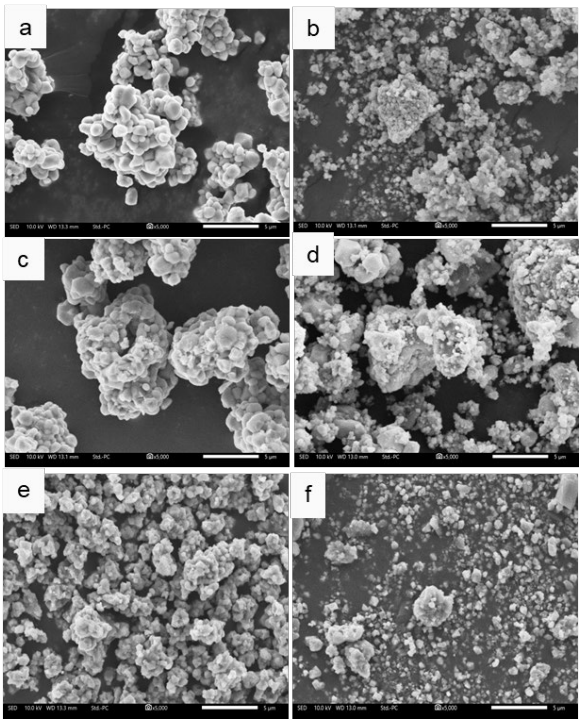

Fig. 4. SEM NMC622 Images with Various Doping at 5000x magnification (a. Fe, b. Ti, c. Zn, d. Ce, e. Cu, f. Mg)

Fig. 4 and Fig. 5 show SEM results from various NMC622 particles being doped at magnifications of 5000 and 10000. All samples consist of primary particles and secondary particles. Based on Table 2, all materials have an average primary particle size of less than 0.5 micrometers in the range of 0.1571-1.0153 micrometers. NMC622 with Ce doping has a smaller primary particle size. As is well known, primary particle size seems to have more effect on the surface layer between the active material and electrolytes, and a low interface area can inhibit Li^+ diffusion rates[43]. The size of the secondary polyhedral particle is about 1-4 micrometers.

Secondary particles are agglomerates of primary particles. From the size analyzed using SEM can be seen that metal doping on NMC622 material have given effect to make the material smaller that is better in the point of Li ion diffusion rates.

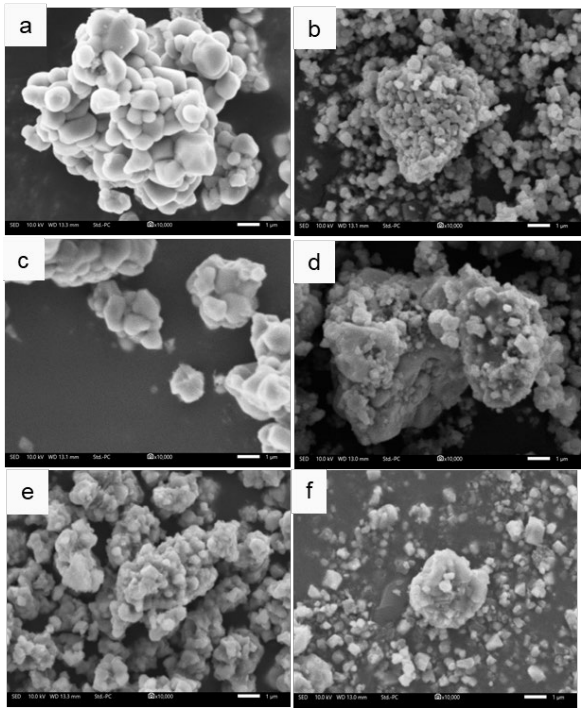

Fig. 5. SEM NMC622 Images with Various Doping at 10000x magnification (a. Fe, b. Ti, c. Zn, d. Ce, e. Cu, f. Mg)

To find out if doping successfully conducted SEM EDX tests on NMC622 material without doping and NMC622 with Fe doping. The material composition data that was successfully synthesized is found in Table 3. Fe doping material was detected in NMC622 material with a percentage of 3.82%.

Table 3. Molar Fraction NMC622 Without Doping and NMC622 Fe

Sample	Element			
	Ni (%)	Mn (%)	Co (%)	Fe (%)
NMC Without Doping	61.748	18.238	20.013	-
NMC622 Fe	57.530	18.914	19.729	3.825

The non-conforming composition of Fe obtained due to several factors including the lack of perfect solid-state process and EDX testing factors are less effective compared to XRF. The composition of Mn is less due to

the process of mixing the smallest Mn solubility compared to Ni and Co.

Fig. 6 shows NMC622 cathode charge- capability with various doping conditions in the voltage range of 2.6 V-4.3 V using a current of 0.1 C. NMC622 without doping has the highest capacity of 70 mAh/g then NMC622 with Ce doping has a higher specific release capacity compared to other metal doping which is 64 mAh/g.

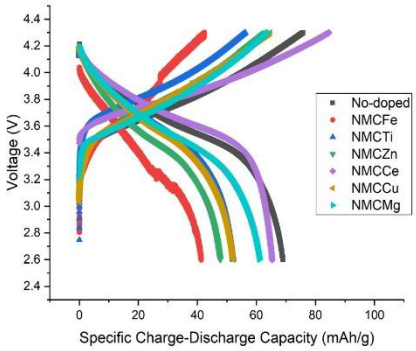

Fig. 6. NMC622 Charge-Discharge Performance with Various Doping

In addition, in the results of the characterization of FTIR material NMC622 with doping Ce was found to have no O-H phase and little CO3 phase indicating that NMC622 material was perfectly formed. Lower value of specific capacity caused by change in parameter c associated with hexagonal H3 phase formation nearing end of charging 47).

Fig. 7 shows charge-discharge testing of NMC622 without doping and NMC622 with Ce doping. NMC622 without doping reaches a capacity of 70 mAh/g with an energy density of 247 mWh/g while NMC622 with Ce doping has a capacity of 64 mAh/g with an energy density of 240 mWh/g. The energy obtained is almost the same however, NMC622 with Doping Ce reaches a higher average voltage than NMC622 without doping which is 3.75V while NMC without doping is 3.67V. During its lifespan, an ideal lithium-ion cell should have a constant average charge voltage and a constant average discharge voltage[48]. From the Fig.7 shown that the NMC with Ce doping (red line) has a better constant voltage than the NMC without doping.

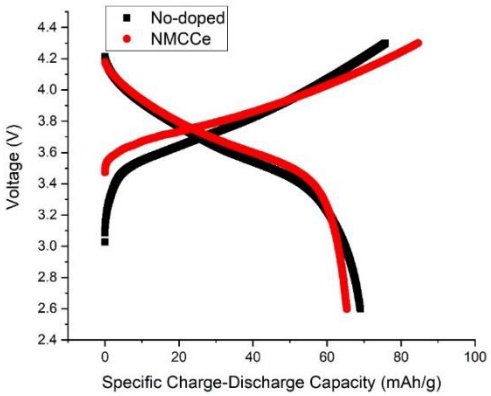

Fig. 7. Charge-Discharge Performance from NMC622 Ce and NMC622 Without Doping

However, after 3.2V NMC with doping Ce had a more dominant diffusion phase which led to a lower specific discharge capacity. Diffusion phase or concentration polarization is affected by the unavailability of active species on the electrode/electrolyte interface to continue the reaction. During the reaction, the active species particles must diffuse to the surface of the electrode to replace the material that previously reacted[49]. NMC with Doping Ce began to run out of active species at voltages of 3.2V.

However, due to the cathode structure fluctuates based on the re-conversion reaction during each filling and discharge operation, the cathode efficiency is highly dependent on treatments such as electrode material mixing, current rate, and temperature[50]. On NMC622 batteries with Doping Ce conducted cycle tests at a rate of 0.1C and showed no significant decrease as seen in Fig. 8. When compared to NMC622 without doping, the decrease in capacity in the first 4 cycles is smaller. The decrease in capacity of NMC622 without doping after 4 cycles was 88.7% moderate with Ce doping capacity reduction after 4 cycles was 96.63%. The decrease in capacity suggests that with Ce doping can help stabilize the NMC622 battery cycle. The presence of CeO_2 group on the material helps in the process of stabilizing the material as Wu (2009) has done on the NMC111 battery.

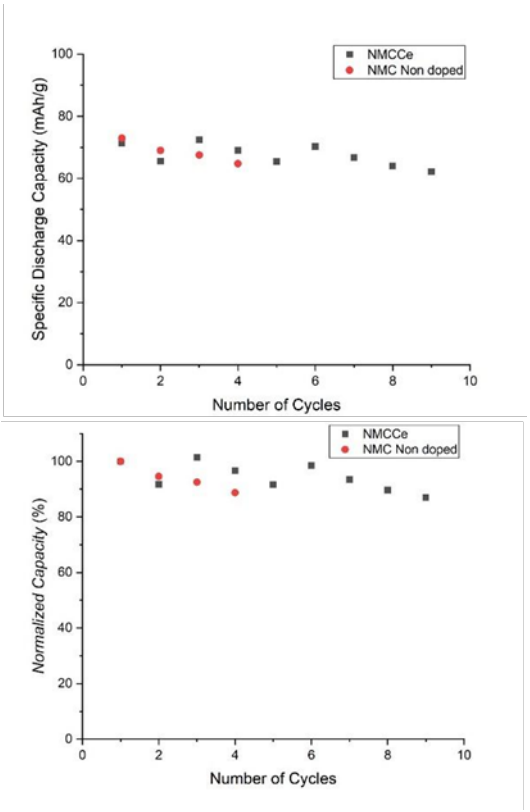

Fig. 8. NMC622 Ce and NMC622 Cycle Tests without Doping

EIS analysis is conducted at a frequency range of 8000 – 0.01 Hz on batteries with 3 charge-discharge cycles. EIS analysis done to find the ion conductivity of the electrolyte. In order to assess a material's ability to accommodate electric current, its conductivity must be determined. This is in relation to the charge or ion conductivity of a battery electrode material[51].

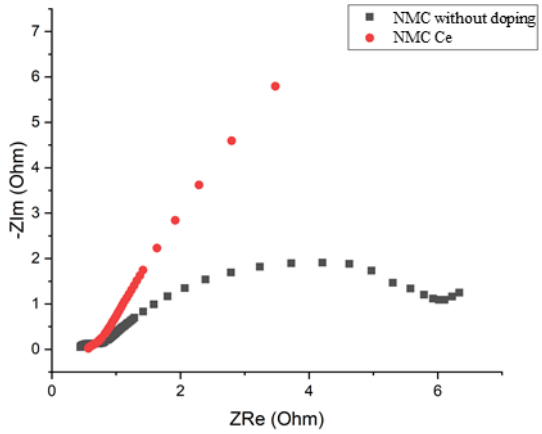

Fig. 9. Nyquist Plot

Nyquist diagrams in Fig. 9 of NMC622 batteries without doping and NMC622 with Ce doping depicting an imaginary impedance plot against real impedance. NMC622 with Ce doping has not formed semicircle yet while NMC622 without doping formed 2 semicircles at high frequencies and warburg phase at low frequencies. Nyquist's plot shows the inductive phase at high frequencies, followed by two semicircles and a typical Warburg phase at the lowest frequency [52]. There are two semicircles for further investigation, and the Warburg phase use the analogous circuit model depicted in Fig. 9.

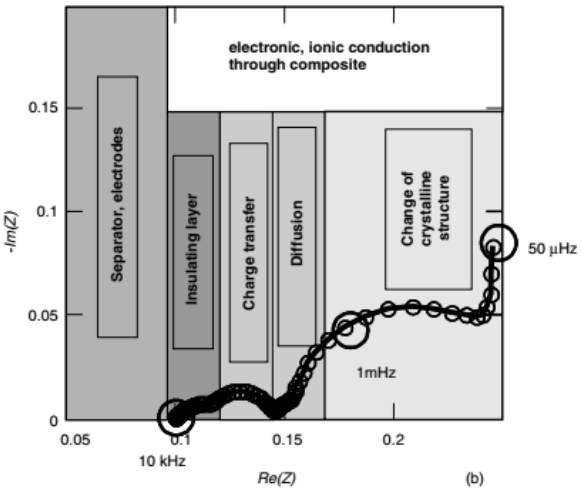

Fig. 10. Spectra Impedance Intercalation Material on Battery (Reprinted with permission from ref [53]. Copyright 2005 A John Wiley & Sons, Inc.)

The spectra impedance model in Fig. 10 is often used in the literature to describe a battery-filled cell. At the highest frequencies, signals are dominated by inductive phenomena arising from the impedance measurement environment. Electronic inductance and resistance elements, considered primarily arising from electrolyte resistance, which are a side influence of assembly processes, such as cell tabs, welding points, impedance channel contacts and cables. In Fig. 9, the first semicircle represents the phenomenon of surface resistance. The second semicircle is driven by a charge transfer reaction from graphite anode and NMC cathode. After the semicircle, the diagonal line is the diffusion phase represented by the Warburg phase. Cathode NMC622 with doping Ce there is only the Warburg phase which is also supported with Fig. 7. However, because of the large ion concentrations present in charge-discharge reactions and the relatively thin electrolyte coatings used in batteries, such impedance can be ignored for most liquid electrolytes used in practice, and their impact will only be seen at high frequencies[53].

4. Conclusion

The NMC622 cathode was successfully synthesized via direct co-precipitation technique, and the electrochemical performance and structural impacts of doping were investigated. Dopants have an influence on particle size and stability, according to structural investigations. The initial discharge capability of the active materials in the all metal doped NMC622 cathode

was lower than theoretical un-doped NMC. A reduction in specific capacity is caused by a change in the c parameter associated with the creation of the hexagonal H3 phase at the conclusion of charging. The influence of transition metal doping composition in NMC622 cathode material is different for each metal. NMC622 cathode material with transition metal doping has crystalline structure characteristics similar to NMC622 cathode material without doping, but for morphology and particle size differs from NMC622 material without doping. In electrochemical tests, it was obtained that NMC622 with Ce doping has almost the same capacity as NMC622 without doping with the same synthesis process and has better early cycle stability compared to NMC622 without doping. In the future, further effort will be necessary to achieve a greater and more dependable discharge capacity.

Acknowledgements

Through the Pendanaan Riset Inovatif Produk (Rispro) Invitasi grant no.PRJ-6/LPDP/2020, the Indonesia Endowment Fund for Education (Lembaga Pengelola Dana Pendidikan/ LPDP) has supported this study. PT Pertamina, under contract number 007/P00000/2019-S0, has also contributed to this publication.

Conflict of Interest

There are no conflicts of interest between authors.

References

1) Y.L. Ding, Z.P. Cano, A. Yu, J. Lu, and Z. Chen, "Automotive li-ion batteries: current status and future perspectives," *J. Chem. Inf. Model.*, **53** (*9*) 1689–1699 (1981).
2) K. Chihara, M. Ito, A. Kitajou, and S. Okada, "Cathode property of na2cxox [x = 4, 5, and 6] and k2c6o6 for sodium-ion batteries," *Evergreen*, **4** (*1*) 1–5 (2017). doi:10.5109/1808304.
3) K. Nakamoto, R. Sakamoto, A. Kitajou, M. Ito, and S. Okada, "Cathode properties of sodium manganese hexacyanoferrate in aqueous electrolyte," *Evergreen*, **4** (*1*) 6–9 (2017). doi:10.5109/1808305.
4) A.O. Yurwendra, and L. Noerochim, "Pengaruh konsentrasi karbon terhadap performa elektrokimia katoda lifepo4 untuk aplikasi baterai lithium ion tipe aqueous electrolyte," *Ejurnal.Its.Ac.Id*, **3** (*2*) 4–9 (2014). http://ejurnal.its.ac.id/index.php/teknik/article/view/6682.
5) A. Syifaurrahma, Arnelli, and Y. Astuti, "LiOH/coconut shell activated carbon ratio effect on the conductivity of lithium ion battery anode active material annisa," *Molekul*, **16** (*3*) 235–243 (2021).
6) Y. Astuti, R. Mei, A. Darmawan, and H. Widiyandari, "Enhancement of electrical conductivity of bismuth oxide / activated carbon composite," 1–28 (n.d.).
7) J.R. Dahn, E.W. Fuller, M. Obrovac, and U. von Sacken, "Thermal stability of lixcoo2, lixnio2 and λ-mno2 and consequences for the safety of li-ion cells," *Solid State Ionics*, **69** (*3–4*) 265–270 (1994). doi:10.1016/0167-2738(94)90415-4.
8) A. Nojima, A. Sano, H. Kitamura, and S. Okada, "Electrochemical characterization, structural evolution, and thermal stability of livopo4 over multiple lithium intercalations," *Evergreen*, **6** (*4*) 267–274 (2019). doi:10.5109/2547346.
9) D. Doughty, and E.P. Roth, "A general discussion of li ion battery safety," *Electrochem. Soc. Interface*, **21** (*2*) 37–44 (2012). doi:10.1149/2.F03122if.
10) T. Tsubota, A. Kitajou, and S. Okada, "O3-type na(fe1/3mn1/3co1/3)o2 as a cathode material with high rate and good charge-discharge cycle performance for sodium-ion batteries," *Evergreen*, **6** (*4*) 275–279 (2019). doi:10.5109/2547348.
11) B. Xie, A. Kitajou, S. Okada, W. Kobayashi, M. Okada, and T. Takahara, "Cathode properties of na3mpo4co3 (m = co/ni) prepared by a hydrothermal method for na-ion batteries," *Evergreen*, **6** (*4*) 262–266 (2019). doi:10.5109/2547345.
12) A.R. Nurohmah, C.S. Yudha, M. Rahmawati, S.F.S. Nisa, A. Jumari, H. Widiyandari, and A. Purwanto, "Structural and electrochemical analysis of iron doping in lini0.6-xmn0.2co0.2fexo2 battery," *Evergreen*, **8** (*1*) 82–88 (2021). doi:10.5109/4372263.
13) S. Hildebrand, C. Vollmer, M. Winter, and F.M. Schappacher, "Al2O3, sio2 and tio2 as coatings for safer lini0.8co0.15al0.05o2 cathodes: electrochemical performance and thermal analysis by accelerating rate calorimetry," *J. Electrochem. Soc.*, **164** (*9*) A2190–A2198 (2017). doi:10.1149/2.0071712jes.
14) H.J. Noh, S. Youn, C.S. Yoon, and Y.K. Sun, "Comparison of the structural and electrochemical properties of layered li[nixcoymnz]o2 (x = 1/3, 0.5, 0.6, 0.7, 0.8 and 0.85) cathode material for lithium-ion batteries," *J. Power Sources*, **233** 121–130 (2013). doi:10.1016/j.jpowsour.2013.01.063.
15) M. Eilers-Rethwisch, S. Hildebrand, M. Evertz, L. Ibing, T. Dagger, M. Winter, and F.M. Schappacher, "Comparative study of sn-doped li[ni0.6mn0.2co0.2-xsnx]o2 cathode active materials (x = 0-0.5) for lithium ion batteries regarding electrochemical performance and structural stability," *J. Power Sources*, **397** (*January*) 68–78 (2018). doi:10.1016/j.jpowsour.2018.06.072.
16) M. Dixit, B. Markovsky, D. Aurbach, and D.T. Major, "Unraveling the effects of al doping on the electrochemical properties of lini0.5co0.2mn0.3o2using first principles," *J. Electrochem. Soc.*, **164** (*1*) A6359–A6365 (2017). doi:10.1149/2.0561701jes.
17) J.D. Wilcox, E.E. Rodriguez, and M.M. Doeff, "The impact of aluminum and iron substitution on the structure and electrochemistry of li (ni0.4 co0.2-y my mn0.4)o2 materials," *J. Electrochem. Soc.*, **156** (*12*) 1011–1018 (2009). doi:10.1149/1.3237100.

18) M. Iftekhar, N.E. Drewett, A.R. Armstrong, D. Hesp, F. Braga, S. Ahmed, and L.J. Hardwick, "Characterization of aluminum doped lithium-manganese rich composites for higher rate lithium-ion cathodes," *J. Electrochem. Soc.*, **161** (*14*) A2119–A2116 (2014). doi:10.1149/2.0441414jes.
19) Y.X. Wang, K.H. Shang, W. He, X.P. Ai, Y.L. Cao, and H.X. Yang, "Magnesium-doped li<inf>1.2</inf>[co<inf>0.13</inf>ni<inf>0.13</inf >mn<inf>0.54</inf>]o<inf>2</inf> for lithium-ion battery cathode with enhanced cycling stability and rate capability," *ACS Appl. Mater. Interfaces*, **7** (*23*) 13014–13021 (2015). doi:10.1021/acsami.5b03125.
20) W. Cho, J.H. Song, K.W. Lee, M.W. Lee, H. Kim, J.S. Yu, Y.J. Kim, and K.J. Kim, "Improved particle hardness of ti-doped lini1/3co1/3mn1/3-xtixo2 as high-voltage cathode material for lithium-ion batteries," *J. Phys. Chem. Solids*, **123** (*August*) 271–278 (2018). doi:10.1016/j.jpcs.2018.08.008.
21) J. Mao, K. Dai, M. Xuan, G. Shao, R. Qiao, W. Yang, V.S. Battaglia, and G. Liu, "Effect of chromium and niobium doping on the morphology and electrochemical performance of high-voltage spinel lini0.5mn1.5o4 cathode material," *ACS Appl. Mater. Interfaces*, **8** (*14*) 9116–9124 (2016). doi:10.1021/acsami.6b00877.
22) B. Pişkin, C. Savaş Uygur, and M.K. Aydınol, "Mo doping of layered li (nixmnyco1-x-y-zmz)o2 cathode materials for lithium-ion batteries," *Int. J. Energy Res.*, **42** (*12*) 3888–3898 (2018). doi:10.1002/er.4121.
23) M. Eilers-Rethwisch, M. Winter, and F.M. Schappacher, "Synthesis, electrochemical investigation and structural analysis of doped li[ni 0.6 mn 0.2 co 0.2-x m x]o 2 (x = 0, 0.05; m = al, fe, sn) cathode materials," *J. Power Sources*, **387** (*January*) 101–107 (2018). doi:10.1016/j.jpowsour.2018.02.080.
24) S. Park, D. Kim, H. Ku, M. Jo, S. Kim, J. Song, J. Yu, and K. Kwon, "The effect of fe as an impurity element for sustainable resynthesis of li[ni1/3co1/3mn1/3]o2 cathode material from spent lithium-ion batteries," *Electrochim. Acta*, **296** 814–822 (2019). doi:10.1016/j.electacta.2018.11.001.
25) X. Cheng, H. Wei, W. Hao, H. Li, H. Si, S. An, W. Zhu, G. Jia, and X. Qiu, "A cobalt-free li(li 0.16 ni 0.19 fe 0.18 mn 0.46)o 2 cathode for lithium-ion batteries with anionic redox reactions," *ChemSusChem*, **12** (*6*) 1162–1168 (2019). doi:10.1002/cssc.201802436.
26) H. Li, H. Guo, Z. Wang, J. Wang, X. Li, N. Chen, and W. Gui, "Improving rate capability and decelerating voltage decay of li-rich layered oxide cathodes by chromium doping," *Int. J. Hydrogen Energy*, **43** (*24*) 11109–11119 (2018). doi:10.1016/j.ijhydene.2018.04.203.
27) Li H, Cormier M, Zhang N, et al (2019) Is Cobalt Needed in Ni-Rich Positive Electrode Materials for Lithium Ion Batteries? *J Electrochem Soc,* **166**:A429–A439. https://doi.org/10.1149/2.1381902jes
28) N.H.S. Nasralla, M. Yeganeh, Y. Astuti, S. Piticharoenphun, and L. Šiller, "Systematic study of electronic properties of fe-doped tio2 nanoparticles by x-ray photoemission spectroscopy," *J. Mater. Sci. Mater. Electron.*, **29** (*20*) 17956–17966 (2018). doi:10.1007/s10854-018-9911-5.
29) S. Wolff-Goodrich, F. Lin, I.M. Markus, D. Nordlund, H.L. Xin, M. Asta, and M.M. Doeff, "Tailoring the surface properties of lini0.4mn0.4co0.2o2 by titanium substitution for improved high voltage cycling performance," *Phys. Chem. Chem. Phys.*, **17** (*34*) 21778–21781 (2015). doi:10.1039/c5cp03228h.
30) I.M. Markus, F. Lin, K.C. Kam, M. Asta, and M.M. Doeff, "Computational and experimental investigation of ti substitution in li1(nixmnxco1-2x-ytiy)o2 for lithium ion batteries," *J. Phys. Chem. Lett.*, **5** (*21*) 3649–3655 (2014). doi:10.1021/jz5017526.
31) H. Du, Y. Zheng, Z. Dou, and H. Zhan, "Zn-doped lini1/3co1/3mn1/3o2 composite as cathode material for lithium ion battery : preparation , characterization , and electrochemical properties," *Jounal Nanomater.*, **2015** (*Cv*) 1–6 (2015).
32) E.R. Dyartanti, I.N. Widiasa, A. Purwanto, and H. Susanto, "Nanocomposite polymer electrolytes in pvdf/zno membranes modified with pvp for use in lifepo4 batteries," *Evergreen*, **5** (*2*) 19–25 (2018). doi:10.5109/1936213.
33) F. Wu, M. Wang, Y. Su, L. Bao, and S. Chen, "Surface of lico1/3ni1/3mn1/3o2 modified by ceo2-coating," *Electrochim. Acta*, **54** (*27*) 6803–6807 (2009). doi:10.1016/j.electacta.2009.06.075.
34) L. Yang, F. Ren, Q. Feng, G. Xu, X. Li, Y. Li, E. Zhao, J. Ma, and S. Fan, "Effect of cu doping on the structural and electrochemical performance of lini1/3co1/3mn1/3o2 cathode materials," *J. Electron. Mater.*, **47** (*7*) 3996–4002 (2018). doi:10.1007/s11664-018-6284-8.
35) M. Lou, S.S. Fan, H.T. Yu, Y. Xie, Q. Zhang, Y.R. Zhu, T.F. Yi, and G.H. Tian, "Mg-doped li1.2mn0.54ni0.13co0.13o2 nano flakes with improved electrochemical performance for lithium-ion battery application," *J. Alloys Compd.*, **739** 607–615 (2018). doi:10.1016/j.jallcom.2017.12.286.
36) Q. Li, G. Li, C. Fu, D. Luo, J. Fan, J. Zheng, D. Xie, and L. Li, "A study on storage characteristics of pristine li-rich layered oxide li1.20mn0.54co0.13ni0.13o2: effect of storage temperature and duration," *Electrochim. Acta*, **154** 249–258 (2015). doi:10.1016/j.electacta.2014.12.071.
37) T. Dong, X. Yu, L. Zhang, and P. Yang, "Synthesis and properties of cathode materials xli2mno 3·(1-x)limn1/3ni1/3co 1/3o2 for li-ion batteries," *J. Nanosci. Nanotechnol.*, **14** (*4*) 3041–3045 (2014). doi:10.1166/jnn.2014.8599.

38) C. Cao, L. Xi, K.L. Leung, M. Wang, Y. Liu, R. Ma, S. Yang, Z. Lu, and C.Y. Chung, "Facile synthesis of porous li-rich layered li[li0.2mn0.534ni0.133co0.133]o2 as high-performance cathode materials for li-ion batteries," *RSC Adv.*, **5** (*39*) 30507–30513 (2015). doi:10.1039/c5ra03445k.
39) C. Te Hsieh, H.H. Hsu, J.P. Hsu, Y.F. Chen, and J.K. Chang, "Infrared-assisted synthesis of lithium nickel cobalt alumina oxide powders as electrode material for lithium-ion batteries," *Electrochim. Acta*, **206** 207–216 (2016). doi:10.1016/j.electacta.2016.04.146.
40) W. Yuan, H.Z. Zhang, Q. Liu, G.R. Li, and X.P. Gao, "Surface modification of li(li0.17ni0.2co 0.05mn0.58)o2 with ceo2 as cathode material for li-ion batteries," *Electrochim. Acta*, **135** 199–207 (2014). doi:10.1016/j.electacta.2014.04.181.
41) Y. Liu, R. Li, J. Li, Z. Yang, J. Zhong, Z. Wang, and F. Kang, "A high-performance ce and sn co-doped cathode material with enhanced cycle performance and suppressed voltage decay for lithium ion batteries," *Ceram. Int.*, **45** (*16*) 20780–20787 (2019). doi:10.1016/j.ceramint.2019.07.064.
42) R.J. Gummow, "Lithium intercalation reactions with transition metal oxides," University of Cape Town, 1993. https://open.uct.ac.za/handle/11427/19039.
43) L. Xu, F. Zhou, J. Kong, H. Zhou, Q. Zhang, Q. Wang, and G. Yan, "Influence of precursor phase on the structure and electrochemical properties of li(ni0.6mn0.2co0.2)o2 cathode materials," *Solid State Ionics*, **324** (*April*) 49–58 (2018). doi:10.1016/j.ssi.2018.06.010.
44) J.Z. Kong, H.F. Zhai, C. Ren, M.Y. Gao, X. Zhang, H. Li, J.X. Li, Z. Tang, and F. Zhou, "Synthesis and electrochemical performance of macroporous lini 0.5co0.2mn0.3o2 by a modified sol-gel method," *J. Alloys Compd.*, **577** 507–510 (2013). doi:10.1016/j.jallcom.2013.07.007.
45) A. Jumari, K. Nur, R. Stulasti, R.N. Halimah, L.A. Aini, and R. Mintarsih, "Production of lini0.6mn0.2co0.2.2o2 via fast oxalate precipitation for li-ion," *AIP Conf. Proc.*, **030011** (*April*) 2–7 (2020). doi:https://doi.org/10.1063/5.0000646.
46) M. Arinawati, A.P. Hutama, C.S. Yudha, M. Rahmawati, and A. Purwanto, "Facile rheological route method for lifepo4/c cathode material production," *Open Eng.*, **11** (*1*) 669–676 (2021). doi:10.1515/eng-2021-0068.
47) T. Weigel, F. Schipper, E.M. Erickson, F.A. Susai, B. Markovsky, and D. Aurbach, "Structural and electrochemical aspects of lini 0.8 co 0.1 mn 0.1 o 2 cathode materials doped by various cations," *ACS Energy Lett.*, **4** (*2*) 508–516 (2019). doi:10.1021/acsenergylett.8b02302.
48) J.E. Harlow, S.L. Glazier, J. Li, and J.R. Dahn, "Use of asymmetric average charge- and average discharge- voltages as an indicator of the onset of unwanted lithium deposition in lithium-ion cells," *J. Electrochem. Soc.*, **165** (*16*) A3595–A3601 (2018). doi:10.1149/2.0011816jes.
49) P.P. Mukherjee, "Overdischarge and external short behavior of lithium-ion batteries," (*May*) (2017).
50) K. Hashizaki, S. Dobashi, S. Okada, T. Hirai, J.I. Yamaki, and Z. Ogumi, "Charge-discharge characteristics of li/cucl2 batteries with lipf6/methyl difluoroacetate electrolyte," *Evergreen*, **6** (*1*) 1–8 (2019). doi:10.5109/2320995.
51) Y. Astuti, H. Widiyandari, F.A. Zaqia, L. Annisa, R.M. Fajarwati, and S. Hartinah, "Physicochemical characteristics and electrical conductivity of bismuth oxide/activated carbon composite," *IOP Conf. Ser. Mater. Sci. Eng.*, **1053** (*1*) 012014 (2021). doi:10.1088/1757-899x/1053/1/012014.
52) M. Frankenberger, M. Singh, A. Dinter, and K.H. Pettinger, "EIS study on the electrode-separator interface lamination," *Batteries*, **5** (*4*) (2019). doi:10.3390/batteries5040071.
53) E. Barsoukov, and J.R. Macdonald, "Impedance Spectroscopy Theory, Experiment, and Applications," Second, A John Wiley & Sons, Inc., Publication, 2005.